One-step non-hydrolytic sol-gel synthesis of mesoporous SiO2-Al2O3-NiO catalysts for ethylene oligomerization

Atheer Al Khudhair, Karim Bouchmella, Radu Dorin Andrei, Ahmad Mehdi, P. Hubert Mutin, Vasile Hulea

One-step non-hydrolytic sol-gel synthesis of mesoporous SiO_2-Al_2O_3-NiO catalysts for ethylene oligomerization

Atheer Al Khudhair,[a,b] Karim Bouchmella,[a*] Radu Dorin Andrei,[a,c] Ahmad Mehdi,[a] P. Hubert Mutin,[a] and Vasile Hulea[a]

[a] ICGM, Univ Montpellier, CNRS, ENSCM, Montpellier, France

[b] Department of Chemistry, College of Science, University of Kerbala, 56001 Karbala, Iraq

[c] National Research and Development Institute for Cryogenic and Isotopic Technologies, ICSI Energy Department, Râmnicu Vâlcea, Romania

* Corresponding author, email: karim.bouchmella@umontpellier.fr

Abstract

Mesoporous SiO_2-Al_2O_3-NiO mixed oxide catalysts with different Si/Al ratio and a Ni content of ≈5.5 wt% have been prepared by a simple, one-step non-hydrolytic sol-gel route and evaluated in the oligomerization of ethylene. The catalysts were characterized by TEM-EDX, N_2-physisorption, NH_3-TPD, powder XRD, ^{29}Si and ^{27}Al MAS-NMR, XPS, and H_2-TPR. The Si/Al ratio was found to influence both the texture and the acidity of the materials. According to XRD, part of the Ni formed NiO crystallites, but according to XPS, no bulky NiO was detected at the surface of the catalysts. XPS spectra and TPR experiments are consistent with the formation of dispersed Ni^{2+} species strongly interacting with the surface. The samples with high Al content displayed excellent performances with very high specific activity up to 270 mmol ethylene converted per g of catalyst per hour at 150 °C, and a percentage of butenes in the products of ≈70%. These catalysts compare well with model catalysts prepared by time-consuming multistep procedures from expensive ordered mesoporous silica supports.

Keywords

Non-hydrolytic sol-gel; non-aqueous sol-gel; heterogenous catalysis; olefin oligomerization; mixed oxides.

Introduction

Ethylene oligomerization is one of the major technologies for producing higher olefins, which are key feedstock in the synthesis of plastics, lubricants, surfactants, alcohols, etc. The current oligomerization processes use organic solvents and homogeneous catalysts [1-3]. In line with sustainable chemistry principles, significant research efforts have been directed to the development of heterogeneous catalysts and processes [3-5].Various families of solid catalysts, including complexes immobilized on polymers and oxides, metal-organic framework and covalent organic framework materials, and nickel supported on inorganic porous materials, have been examined during the past decades [3,5]. Among them, Ni-containing zeolites, clays and mesoporous aluminosilicates have shown very promising performances in terms of catalytic activity and selectivity [3,4,6]. In addition, they are the only catalysts that can function without solvents and activators/co-catalyst.

These Ni-containing catalysts are actually bifunctional catalysts, containing both nickel ions and acid sites. It is generally admitted that the isolated nickel ions are involved in the formation of 1-olefins by ethylene dimerization/oligomerization, while the acid sites catalyze the double bond isomerization and the co-oligomerization of primary olefins. These reactions lead to a mixture of C4-C6-C8-… olefins, the composition of which also depends on the reaction conditions (temperature, pressure, contact time) [5,7,8].

The performances of the oligomerization catalysts strongly depend on their textural properties. In a general manner, the activity increases when the pore size of the catalyst increases. The best performances were obtained over catalysts based on nickel-exchanged aluminated ordered mesoporous silicas, namely Ni/Al-MCM-41 [9-11], Ni/Al-SBA-15 [12], and Ni/Al-MCM-48 [13]. The mesoporosity of these catalysts facilitate the diffusion of higher

product molecules inside the pore system, leading to a lower deactivation rate and a higher activity in comparison with the microporous catalysts.

However, the preparation of these model catalysts is time-consuming and energy intensive. For instance, the preparation of Ni/Al-SBA-15 [12], considered to be one of the most active and stable oligomerization catalyst [3], involves three successive steps (synthesis of the ordered silica in the presence of a copolymer template, alumination with $NaAlO_2$, Ni deposition by a two-step exchange procedure), each of them followed by a calcination treatment. On the other hand, the non-hydrolytic sol-gel process based on the reaction of silicon or metal precursors with an organic oxygen donor (ether, alcohol, or alkoxide) offers straightforward one-step routes to non-ordered mesoporous oxides [14]. This process has been successfully applied to the synthesis of mixed oxide catalysts [15], including TiO_2-V_2O_5 DeNOx [16] or total oxidation catalysts [17], SiO_2-TiO_2 epoxidation catalysts [18,19], or SiO_2-Al_2O_3-MO_x (M = Mo, Re) metathesis oxides catalysts [20,21]. Recent reviews show that non-hydrolytic sol-gel is still attracting increasing attention for the preparation of catalysts [22,23].

In this work, we report the first non-hydrolytic sol-gel synthesis of mesoporous NiO-SiO_2-Al_2O_3 catalysts. Mixed oxides with different Si/Al ratios and a Ni content of ≈5.5 wt% were prepared in one step by reaction of nickel bis(acetylacetonate), silicon tetrachloride and aluminium trichloride precursors with diisopropyl ether at 110 °C, followed by calcination in air. Despite this very simple synthesis, the catalytic performance in ethylene oligomerization of these sol-gel mixed oxides compare well with those of a Ni/Al-SBA-15 (2.6 wt% Ni) model catalyst.

2. Experimental section

2.1. Synthesis of the catalysts

The SiO_2-Al_2O_3-NiO mixed oxides with different Si/Al ratios (0, 0.1, 1, 8, ∞) and a Ni content of ≈5.5 wt% were synthesized using silicon tetrachloride ($SiCl_4$, Alfa Aesar, 99.98%), aluminum trichloride ($AlCl_3$, Alfa Aesar, 99.98%) and nickel bis(acetylacetonate) ($Ni(acac)_2$, Alfa Aesar, 95%) as molecular precursors. $Ni(acac)_2$ was used instead of $NiCl_2$ because of its better solubility in the experimental conditions. Dry diisopropyl ether (iPr_2O, H_2O < 4 ppm) and CH_2Cl_2 (H_2O < 6 ppm) used as oxygen donor and solvent, respectively, were purchased from Aldrich with 99 % purity and were further dried by distillation over sodium wire. The water concentration was determined by the method of assaying water using Karl Fisher reagent (Metrohm KF 652 coulometric type). The catalysts were prepared in 1 g quantities in 48 mL PTFE lined autoclaves (Parr Instruments). All manipulations were performed under argon using a glovebox to avoid hydrolysis. The chloride and acetylacetonate precursors were introduced first in the autoclave, then iPr_2O and CH_2Cl_2 (10 mL) were added. The number of moles of iPr_2O was calculated so that the number of iPr groups in iPr_2O was equal to the total number of Cl and acac groups in the precursors. The sealed autoclave was heated at 110 °C for 4 days under autogenous pressure. In this synthesis, the reactions around Si are catalyzed by $AlCl_3$. In the preparation of the Al-free mixed oxide (Si/Al = ∞), $FeCl_3$ (0.015 mmol) had to be used as a catalyst to obtain a gel. After cooling down to room temperature, the gel was washed (under air atmosphere) with CH_2Cl_2, dried at 20 °C under vacuum (10 Pa) for 1 h and then for 4 h at 120 °C. The resulting xerogel was crushed in a mortar and calcined in air at 500 °C for 5h (heating rate 10 °C min^{-1}). The samples are labeled $Si_xAl_yNi_z$, where x, y and z represent the nominal SiO_2, Al_2O_3 and NiO weight loadings, respectively. The overall oxide yield was better than 90 % in all cases. The as-prepared materials appeared either as fine powders (more than 45 wt % of Al_2O_3) or as coarse powders with larger particle sizes (less than 45 wt % of Al_2O_3).

2.2. Characterization

The atomic percentages of Ni, Si and Al were obtained by energy dispersive X-ray spectroscopy (EDX). Measurements were carried out using an X-Max Silicon Drift detector mounted on an FEI Quanta FEG 200 scanning electron microscope. To obtain reliable results in the analyses, the data for each sample is the average of three separate measurements. The use of a piece of Scotch® to fix the powder and the partial vacuum (0.3 Torr) in the measuring chamber does not allow for a correct analysis of the concentrations in C and O. SEM images were obtained using a JEOL 1200 EX II (120 kV) microscope. X-ray powder diffractograms (XRD) were obtained on a Philips X-pert Pro II diffractometer using Kα copper Cu radiation (λ = 1.5418 Å) as a radiation source. The diffractograms were obtained in the range 2θ from 20 to 80 ° in steps of 0.02 °. Transmission electronic microscopy (TEM) was carried out with a JEOL 2200 FS instrument (0.23 nm point-to-point resolution) with an accelerating voltage of 200. The solid-state $^{1}H \rightarrow ^{29}Si$ CP-MAS NMR spectra were recorded on a 59.6 MHz VARIAN VNMRS 300 spectrometer with a MAS (magic angle spinning) probe and 7.5 mm zirconia rotors, using a cross-polarization sequence (CP) with a 3 ms contact time, a 5 s recycling delay and a 5 kHz spinning frequency. Chemical shifts were referenced to tetramethylsilane using octa(dimethylsiloxy)silsesquioxane $Q_8M^H_8$ as a secondary reference. The solid-state ^{27}Al NMR spectra were recorded on a 104.26 MHz VARIAN VNMRS 400 spectrometer with a MAS (magic angle rotation) probe with 3.2 mm zirconia rotors, using a single pulse sequence with ^{1}H decoupling, pulses of 1 µs (corresponding to a pulse angle of π / 12), a recycling time of 1 s and a spinning frequency of 20 kHz. The chemical shifts were referenced with respect to an aqueous solution of aluminum nitrate. N_2 physisorption experiments were performed at 77 K on a Tristar instrument from Micromeritics. The calcined samples were outgassed overnight at 150 °C under vacuum (2 Pa). The specific surface area (S_{BET}) was determined by the BET method in the 0.05 to 0.30

P/P_0 range. The total pore volume V_P was measured at P/P_0 = 0.985. The average pore diameter D_P was calculated from the total pore volume and the specific surface area ($D_P = 4 V_P/ S_{BET}$). The pore size distribution was derived from the desorption branch using the BJH method. The total volume of the micropores of the samples was estimated by the *t*-plot analysis. The acidity was evaluated by temperature programmed desorption of ammonia (NH_3-TPD) on a Micromeritics AutoChem 2910 apparatus with a thermal conductivity detector. The sample (100 mg) was preheated in helium at 200 °C for 60 min (heating rate 10 °C min^{-1}). Adsorption of NH_3 (pure ammonia, flow rate 30 ml min-1) was done at 100 °C for 60 min. Physisorbed NH_3 was removed by purging with helium at 100 °C for 1 h (flow rate 30 ml min^{-1}). The TPD measurement was conducted by heating the sample from 100 to 650 °C at a 10 °C min^{-1} heating rate. The relative amounts of weak and medium-strong sites were estimated using the method described by Katada et al.[24] A Gaussian function centered at *ca.* 180 °C was fitted to the peak and attributed to weak acid sites. The rest of the peak was attributed to medium and strong acid sites. Temperature programmed reduction (H_2-TPR) analyses of the samples was carried out using a Micromeritics AutoChem 2910 apparatus, equipped with a thermal conductivity detector (TCD). For the pretreatment, the sample (140 mg) was placed in a U-shaped quartz tube then heated up to 500 °C (heating rate 10 °C min^{-1}) in He for 1h, then cooled down to 25 °C. The TPR was carried out using H_2/He (25/75, v/v) at a flow rate of 13 cm^3 min^{-1}. The temperature was increased from 25 to 600 °C at a heating rate of 10 °C min^{-1}. The tail gas was directly passed to the TCD to determine the hydrogen consumption in the gas stream.

X-ray photoelectron spectroscopy (XPS) was performed on an Electron ESCALAB 250 spectrometer using the monochromatic source, line Al Kα (1486.6 eV) as excitation source, which was operated in the constant-pass energy mode. The pressed sample in small stainless steel troughs of 4 mm diameter was placed on a ceramic carousel. The pressure in the analysis

chamber was around 10^{-6} Pa. The angle between the surface normal and the axis of the analyzer lens was 55 °. The analyzed area was approximately 1.4 mm^2 and the pass energy was set at 150 eV. In these conditions, the resolution determined by the full width at half maximum (FWHM) of the Au 4f7/2 peak was around 1.6 eV. A flood gun set at 10 eV and a Ni grid placed 3 mm above the sample surface was used for charge stabilization. The spectra were referenced using the C1S line of adventitious hydrocarbon fixed at 284.8 eV.

2.3. Catalytic test

The catalytic oligomerization of ethylene was performed in flow mode in a stainless steel fixed bed reactor (i.d.5 mm) in the presence of 0.5 g of catalyst. The inlet flow consisted of pure ethylene, supplied at 3.0 MPa at a controlled feed rate (4 L h^{-1}), corresponding to a mass hourly space velocity (WHSV) of 10 h^{-1}. The pressure was controlled via a backpressure regulator. Activation of the catalyst prior to each test was performed in the reactor at 550 °C for 8h under dinitrogen flow. Catalytic tests were performed sequentially at 150, 200, 250, 300 and 350 °C, holding the reactor at each temperature for 1 h. The complete reactor effluence was analyzed online by gas chromatography (Varian CP- 3800, FID), using a CP-PoraPLOT Q capillary column (25 m, 0.53 mm, 20 μm) and an auto-sampling valve. The specific activity was defined as the number of moles of ethylene converted to oligomerization products (C4, C6 and C8) per gram of catalyst per hour.

3. Results and discussion

3.1. Synthesis and characterization of the catalysts

The SiO_2-Al_2O_3-NiO catalysts were prepared by a one-step non-hydrolytic sol-gel route, involving the reaction at 110 °C under autogenous pressure of $SiCl_4$, $AlCl_3$, and $Ni(acac)_2$ precursors with iPr_2O in CH_2Cl_2. The gels obtained were dried under vacuum then calcined

for 5 h at 500 °C in dry air. Five samples with various Si/Al ratios and a constant Ni content (≈5.5 wt% Ni, corresponding to ≈7 wt% NiO) were prepared (Table 1). The samples are labeled $Si_xAl_yNi_z$, where x, y and z represent the nominal SiO_2, Al_2O_3 and NiO weight loadings, respectively.

The experimental composition of the samples determined by EDX analysis was close to the nominal one based on the amounts of reactants, indicating that all of the Si, Al and Ni atoms were included in the final oxide, as found previously for other mixed oxide catalysts prepared by non-hydrolytic sol-gel [20,21,25,26].

The nitrogen physisorption isotherms of the samples were of type IV, typical of mesoporous solids (Figure S1). The silica-rich samples ($Si_{80}Al_{12}Ni_8$ and $Si_{93}Al_0Ni_7$) exhibited high specific surface areas (590 and 795 $m^2\ g^{-1}$) and pore volumes (1.5 and 2.0 $cm^3\ g^{-1}$), while the other samples displayed only moderate specific surface area (around 360 $m^2\ g^{-1}$) and significantly lower pore volumes (0.3-0.4 $cm^3\ g^{-1}$). (Table 2). The average pore diameter (Dp) ranged between 3.0 and 10.2 nm. *t*-Plot analysis indicated that the surface area developed by micropore walls was low, except for $Si_{42}Al_{50}Ni_8$. Samples with low Al_2O_3 content ($Si_0Al_{93}Ni_7$ and $Si_9Al_{84}Ni_7$), exhibited pores ranged from 2 to 30 nm whereas broader size distribution was observed for $Si_{93}Al_0Ni_7$ (Figure S2). It is seen that these distributions are relatively narrow and located in the 2-5 nm range for the others alumina-rich samples ($Si_{42}Al_{50}Ni_8$ and $Si_{80}Al_{12}Ni_8$).

Temperature programmed desorption of ammonia (NH_3-TPD) was used to probe the acidity of the $Si_xAl_yNi_z$ samples. All samples exhibited a desorption peak at ≈180 °C (maximum temperature) ascribed to weak acid sites and another peak at 300-350 °C ascribed to medium and strong acid sites (Figure S3). The relative amounts of weak and medium-strong sites was estimated using the method of Katada *et al.* [24]. As shown in Table 2, the total acidity as

well as the percentage of medium or strong acid sites increased with the Al content, as previously observed for Si-Al-Re catalysts [21] prepared by non-hydrolytic sol-gel.

^{29}Si and ^{27}Al solid-state NMR gives information on the structure of the aluminosilicate network. The ^{29}Si CP-MAS NMR spectra of Si-containing mixed oxides (Figure 1) showed broad resonances, typical of amorphous materials. In amorphous silicas or alumino silicates, each replacement of a (OSi) group in $Si(OSi)_4$ tetrahedra by an (OAl) or an (OH) group leads to a downfield shift of about 5 to 10 ppm [27]. The spectrum of $Si_{93}Al_0Ni_7$ shows three broad resonances at ≈-111, -101 and -91 ppm ascribed to $Si(OSi)_4$ (Q^4), $Si(OSi)_3(OH)$ (Q^3), and $Si(OSi)_2(OH)_2$ (Q^2) sites, respectively [28]. It must be noted that the CP-MAS sequence favors Si nuclei close to protons, thus these spectra cannot be used to quantify the concentration of each site. Similar ^{29}Si CP-MAS NMR spectra with a major Q^3 resonance have been reported for mesoporous silicas or silica-alumina with a low Al content [29,30]. The Ni content is too low to have a significant effect (Si/Ni = 16.5), and $Si(OSi)_3(O^-)$ sites bonded to Ni^{2+} cations would lead to a resonance in the -91 to -102 ppm range, thus overlapped by Q^2 and Q^3 resonances [27]. The incorporation of large amounts of aluminum in the silica network led to a significant low-field shift of the resonances indicating extensive formation of Si-O-Al bridges in $Si(OSi)_{4-x}(OAl)_x$(Q^4_{xAl}) sites or $Si(OSi)_{3-x}(OH)(OAl)_x$ (Q^3_{xAl}) sites [27]. Practically all sites from Q^4 sites to Q^4_{4Al} or Q^3_{3Al} sites are likely present in $Si_{42}Al_{50}Ni_8$, while Q^4_{4Al} and/or Q^3_{3Al} sites predominate in $Si_9Al_{84}Ni_7$.

The ^{27}Al solid-state MAS NMR spectra (Figure 2) exhibited broad resonances around 50 ppm, 20 ppm and -10 ppm, ascribed to 4-coordinated (Al^{IV}), 5-coordinated (Al^V), and 6-coordinated (Al^{VI}) aluminum sites [27,31]. The Al^{IV}/Al^{VI} ratio increased from 0.2 to 1.71 when the Si content increased, indicating that the insertion of AlO_4 tetrahedra in the silica network is favored at high Si/Al (Table S1). The signal corresponding to Al^{IV} sites shifted

upfield when the SiO_2 loading increased from 0 to 80 %; this effect has been previously ascribed to the decreased concentration of aluminum atoms around Al sites [32].

According to X-ray diffraction (Figure 3) all samples were predominantly amorphous, but reflections at 2θ = 37.3°, 43.3°, 62.9°, and 76.5° point to the presence of NiO crystallites [33,34], with particle sizes (estimated from the width of the (200) reflection at 43.3°) of ≈25 nm for the alumina-rich samples ($Si_0Al_{93}Ni_7$ and $Si_9Al_{84}Ni_7$) and ≈45 nm for the other samples. Reflections typical of nickel aluminate spinels or of γ-alumina were not detected [35,36]. In the case of $Si_{93}Al_0Ni_7$, a very weak reflection at ≈36 ° could indicate traces of a nickel phyllosilicate phase [37].

Electron microscopy confirmed the formation of NiO crystallites. For instance in the case of $Si_{93}Al_0Ni_7$ TEM images (Figure 4) clearly showed the presence of aggregated, parallelepipedic NiO nanoparticles (with a relatively uniform size of ca. 10-30 nm in width and 20-50 nm in length, in agreement with the crystallite size values estimated from XRD data) dispersed in a porous silica-alumina matrix.

XPS brings additional information on the nature of Ni species. In all cases, the Ni2p3/2 spectra (Figure 5) displayed a main broad peak around 856-857 eV (with a satellite at 862-863 eV) ascribed to tetrahedral Ni^{2+} species in nickel silicate/aluminate domains or to Ni^{2+} species strongly interacting with the aluminosilicate support [38 ,39,40]. The higher binding energy (857.2 eV vs. 856.4 eV) observed for the silica-rich samples suggests a stronger interaction with the support. The silica-rich samples showed an additional peak at 855.3 eV ascribed to octahedral Ni^{2+} species in NiO domains interacting with the support [38-40]. Furthermore, the spectrum of $Si_{80}Al_{12}Ni_8$ showed a signal at ≈853.3 eV corresponding to multiplet splitting characteristic of unsupported NiO, indicating the presence of some bulk NiO at the near surface of this sample [6]. The simple spectra observed for the alumina-rich samples are

similar to those reported for Ni-based catalysts prepared by different methods, such as Ni-exchanged montmorillonite clays,[6] which displayed a peak at 856.9 eV,[6] or NiO–SiO_2–Al_2O_3 catalysts with a 11 wt% Ni content prepared by a hydrolytic sol-gel method with a peak at 856.8 eV [40].

XPS analysis was also used to estimate the concentration of the surface Ni species. In previous works, it was found that when the Tammann temperature of the active phase was sufficiently low (as in the case of V_2O_5, MoO_3, Re_2O_7), calcination led to the migration of the active phase toward the surface [17,20]. The Tammann temperature is the temperature at which ionic diffusion becomes significant in a given material; this temperature roughly corresponds to 0.5 T_f, where T_f is the melting temperature in Kelvin. However, NiO has a very high melting point (1955 °C, 2228 K), which corresponds to a Tammann temperature ~~(0.5 Tf in Kelvin)~~ of 1114 K (841 °C). Accordingly, migration is not expected to occur during calcination at 500 °C. The surface composition obtained from XPS and EDX characterizations is compared in Figure 6. The Ni content detected by XPS was actually lower than by EDX, indicating that the Ni surface concentration was lower than the bulk concentration. A possibility could be that the Ni precursors react faster than Al and Si precursors. This difference in the kinetics of the precursors could lead to a gradient of Ni in the particles building the gel:NiO crystallites formed first and were then embedded in the aluminosilicate matrix. This trend is less pronounced for alumina-rich samples, in agreement with the better dispersion of Ni attested by the smaller size of NiO particles found by XRD.

The reducibility of the nickel species present in each catalyst was examined by TPR reduction with hydrogen up to 900 °C (Figure 7). This technique is classically used to identify the active phases in Ni-based catalysts [11,38,41,42]. Unsupported NiO is reduced at T_{max} ≈350-400 °C (peak maximum), while unsupported $NiAl_2O_4$ is reduced at much higher temperatures, at ≈800-900 °C [38]. In Ni catalysts supported on aluminosilicates, reduction peaks at T_{max}

≈450-600 °C have been ascribed to NiO species strongly interacting with the support or amorphous Ni silicate/aluminate species [33,38,40]; reduction peaks at T_{max} ≈700-800 °C have been attributed to Ni^{2+} charge-compensating cations in aluminosilicates structures [11,42] or to $NiAl_2O_4$ species [33].

The H_2-TPR reduction profiles of $Si_xAl_yNi_z$ catalysts (Figure 7) strongly depend on their composition. The H_2-TPR thermogram of the Al-free $Si_{93}Al_0Ni_7$ sample exhibited a major reduction peak at 400 °C and a shoulder at 470 °C, suggesting that this catalyst contained mainly NiO species with weak interaction with the SiO_2 support. The TPR profiles of all other samples displayed peaks at 500-600 °C implying a significantly stronger interaction of Ni species with the Al-containing matrices. In the case of $Si_{42}Al_{50}Ni_8$ sample, the TPR profile was particularly broad, with a major peak at 650 °C up to 800 °C suggesting the presence of a large amount of $NiAl_2O_4$ species or Ni^{2+} charge-compensating cations in aluminosilicates structures.

3.2. Ethylene oligomerization over $Si_xAl_yNi_z$ catalysts

The catalytic performance measurements were performed in a fixed-bed dynamic reactor, at 150, 200, 250, 300 and 350 °C. Pure ethylene was supplied at 3 MPa with a mass hourly space velocity (WHSV) of 10 h^{-1}. A blank test was performed in the presence of a Ni-free Al-Si mixed oxide (Si/Al = 15) prepared by the non-hydrolytic method; at 150, 200 and 250 °C, the ethylene conversion was only 1, 2 and 5% respectively. In contrast, all $Si_xAl_yNi_z$ samples showed much higher activity (Table 3). This clearly underlines the crucial role played by Ni species in the activation of the ethylene.

The ethylene conversion and the product distribution were highly dependent on the reaction temperature and the composition of the catalyst. As expected, regardless of the composition of the catalyst, the ethylene conversion increased with increasing temperature. Except at the

highest temperature (350 °C), the products were typical of an ethylene oligomerization process catalyzed by Ni-based catalysts. Thus, the main products were C4, C6 and C8 olefins, in which butenes were the major compounds. Small amounts of C1−C3 alkanes and C3, C5, C7 olefins were also obtained, especially at 300 and 350 °C. Figure S4 shows typical chromatograms of the reaction products obtained at different temperatures over the $Si_9Al_{84}Ni_7$ catalyst.

For all of the catalysts, the percentage of C4 olefins decreased when the temperature increased from 150 to 350 °C and the amount of butenes among the products decreased when the Al content in the catalyst increased (Table 3, Figure S5).

This indicates the occurrence of further reactions involving the primary compounds (*vide infra*). In the C4 fraction, the only detected molecules are the three *n*-butene isomers: 1-C4, *trans*-, and *cis*-2-C4. Typically, the distribution of butenes consisted of 17 ± 2% 1-C4, 50 ± 2% *trans*-2-C4, and 33 ± 2% *cis*-2-C4. An exception is the Al-free catalyst, which exhibited the lowest acidity among the catalysts (Table 3). In this case, at 150 °C, the distribution consisted of 40% 1-C4, 31% *trans*-2-C4, and 29% *cis*-2-C4.

The oligomerization results obtained in this study are in agreement with those produced by most of Ni-containing solid catalysts, and confirm the existence of several reactions, as shown in Scheme 1. Ethylene dimerization leading to 1-butene is the primary reaction which occurs on nickel sites. Further oligomerization reactions also occur on nickel sites, leading to 1-hexene then 1-octene. The initial 1-olefins are easily involved in double-bond isomerization reactions. These reactions are favored by the acid properties of the catalyst. The third series of chemical transformations involve the butenes and the hexenes. Known as co-oligomerization reactions, they are also acid-catalyzed reactions. Through an ionic mechanism, the C4 and C6 olefins are converted into branched octenes and higher branched olefins. These reactions are favored by a higher concentration of acid sites as well as a high temperature. Under severe

conditions (i.e. high temperature), the acid sites can also activate cracking and H transfer reactions. The higher selectivity to butenes, as well as the higher 1-butene yield over the $Si_{93}Al_0Ni_7$ catalyst are thus likely related to the lower acidity of this sample.

The results in Table 3 also show the prominent effect of the catalyst composition on ethylene conversion. At 150 °C, the ethylene conversion increased when the amount of aluminum in the catalyst increased, although the specific surface area of the catalysts strongly decreased. At higher reaction temperatures, the most active catalyst was $Si_9Al_{84}Ni_7$ (Figure 8).

The high activity of the alumina-rich catalysts, $Si_0Al_{83}Ni_7$ and $Si_9Al_{84}Ni_7$, cannot be accounted for by a textural effect as these two samples have significantly lower specific surface area than the other samples. XRD indicated the presence in these samples of NiO crystallites of ≈25 nm in size, but XPS suggested that these nanocrystals were not located at the extreme surface of the catalysts. H_2-TPR showed that both catalysts contained a high proportion of Ni sites that reduced at 600 °C, which is quite high for NiO species interacting with a support, and significantly lower than the temperature reported for Ni^{2+} charge-compensating cations in aluminosilicates structures or bulk $NiAl_2O_4$ (>700 °C). Accordingly, the high activity of $Si_0Al_{83}Ni_7$ and $Si_9Al_{84}Ni_7$ might be due to the presence in these catalysts of Ni^{2+} species with a very strong interaction with the alumina/aluminosilicate matrix. These results are consistent with those previously obtained with other Ni-based catalysts.[4,11] It has been shown that the catalytic sites of oligomerization are nickel cations in exchange position and that the oxide species are much less active in this reaction.

To evaluate its stability, $Si_9Al_{84}Ni_8$ was tested over 6 hours at 200 °C (Figure 9). Despite its relatively low pore diameter (3.5 nm) this catalyst appeared fairly stable. After 1 h on stream, it deactivated slowly, with a specific activity decreasing from 324 mmol g^{-1} h^{-1} after 1 h to 275 mmol g^{-1} h^{-1} after 6 h. In addition, the selectivity to butenes and hexenes remained practically constant.

With a specific activity of 271 mmol g^{-1} h^{-1} at 150 °C, 314 mmol g^{-1} h^{-1} at 200 °C, and a selectivity to butenes of 71 % at 150 °C, 66 % at 200 °C, our best catalyst, $Si_9Al_{84}Ni_7$, compares well even with Ni catalysts supported on aluminated ordered mesoporous silicas which are considered the most active heterogeneous oligomerization catalysts. Thus, a Ni/Al-SBA-15 catalyst (Si/Al = 7, 2.6 wt% Ni) tested in flow mode under the exact same conditions exhibited a slightly higher activity: 325 mmol g^{-1} h^{-1}at 150 °C, 343 mmol g^{-1} h^{-1}at 200 °C, but a significantly lower selectivity to butenes: 45% at 150 °C, 38% at 200 °C [12].

Conclusions

In this work, we showed that efficient SiO_2-Al_2O_3-NiO ethylene oligomerization catalysts could be prepared in one step using a non-hydrolytic sol-gel process. This process led to the formation of mesoporous mixed oxides. Depending on the Si/Al ratio, the catalysts can be described as an amorphous silica, aluminosilicate, or alumina matrix embedding NiO nanocrystals; in addition, part of the nickel was dispersed at the surface of the catalyst. The Si/Al ratio influenced the texture and the acidity of the catalysts, as well as the reducibility of Ni species.

The samples with high alumina content were highly active in the ethylene oligomerization of ethylene at 150 or 200 °C, and showed a high selectivity towards butenes and a good stability. Despite their very simple synthesis (one-step, no surfactant, one calcination) these catalysts compared well with the best model oligomerization catalysts reported, Ni-exchanged post-aluminated ordered mesoporous silicas, prepared by time-consuming and energy intensive multistep procedures.

To reach higher catalytic activity, perspectives in the improvement of these materials properties could be the dispersal control of Ni species on the mesoporous aluminosilicate

matrix. In addition, this original sol-gel process could allow experimenters to prepare easily bimetallic catalysts (*e.g.* Ni-Re, Ni-Mo and Ni-W).

Acknowledgements

A.A.K. acknowledges financial support of Iraq Ministry of Higher Education and Scientific Research (MOHESR).

References

[1] C. Bianchini, G. Giambastiani, I.G. Rios, G. Mantovani, A. Meli, A.M. Segarra, Coord. Chem. Rev., 250 (2006) 1391-1418. https://doi.org/10.1016/j.ccr.2005.12.018

[2] D.S. McGuinness, Chem. Rev., 111 (2011) 2321-2341. https://doi.org/10.1021/cr100217q

[3] H. Olivier-Bourbigou, P.A.R. Breuil, L. Magna, T. Michel, M.F. Espada Pastor, D. Delcroix, Chem. Rev., 120 (2020) 7919-7983. https://doi.org/10.1021/acs.chemrev.0c00076

[4] A. Finiels, F. Fajula, V. Hulea, Catal. Sci. Technol., 4 (2014) 2412-2426. https://doi.org/10.1039/C4CY00305E

[5] V. Hulea, ACS Catal., 8 (2018) 3263-3279. https://doi.org/10.1021/acscatal.7b04294

[6] A. Aid, R.D. Andrei, S. Amokrane, C. Cammarano, D. Nibou, V. Hulea, Appl. Clay Sci., 146 (2017) 432-438. https://doi.org/10.1016/j.clay.2017.06.034

[7] S. Moussa, P. Concepción, M.A. Arribas, A. Martínez, ACS Catal., 8 (2018) 3903-3912. https://doi.org/10.1021/acscatal.7b03970

[8] R.D. Andrei, E. Borodina, D. Minoux, N. Nesterenko, J.-P. Dath, C. Cammarano, V. Hulea, Ind. Eng. Chem. Res., 59 (2020) 1746-1752. https://doi.org/10.1021/acs.iecr.9b05576

[9] V. Hulea, F. Fajula, J. Catal., 225 (2004) 213-222. https://doi.org/10.1016/j.jcat.2004.04.018

[10] M. Lallemand, A. Finiels, F. Fajula, V. Hulea, Chem. Eng. J., 172 (2011) 1078-1082. https://doi.org/10.1016/j.cej.2011.06.064

[11] A. Lacarriere, J. Robin, D. Świerczyński, A. Finiels, F. Fajula, F. Luck, V. Hulea, ChemSusChem, 5 (2012) 1787-1792. https://doi.org/10.1002/cssc.201200092

[12] R.D. Andrei, M.I. Popa, F. Fajula, V. Hulea, J. Catal., 323 (2015) 76-84. https://doi.org/10.1016/j.jcat.2014.12.027

[13] M. Lallemand, A. Finiels, F. Fajula, V. Hulea, in: R. Xu, Z. Gao, J. Chen, W. Yan (Eds.), Stud. Surf. Sci. Catal., Elsevier, Beijing, P. R. China, 2007, pp. 1863-1869.

[14] P.H. Mutin, A. Vioux, Chem. Mater., 21 (2009) 582-596. https://doi.org/10.1021/cm802348c

[15] D.P. Debecker, V. Hulea, P.H. Mutin, Appl. Catal., A, 451 (2013) 192-206. http://dx.doi.org/10.1016/j.apcata.2012.11.002

[16] P.H. Mutin, A.F. Popa, A. Vioux, G. Delahay, B. Coq, Appl. Catal., B, 69 (2006) 49-57. https://doi.org/10.1016/j.apcatb.2006.05.021

[17] D.P. Debecker, K. Bouchmella, R. Delaigle, P. Eloy, C. Poleunis, P. Bertrand, E.M. Gaigneaux, P.H. Mutin, Appl. Catal., B, 94 (2010) 38-45. http://dx.doi.org/10.1016/j.apcatb.2009.10.018

[18] O. Lorret, V. Lafond, P.H. Mutin, A. Vioux, Chem. Mater., 18 (2006) 4707-4709. http://dx.doi.org/10.1021/cm061478q

[19] A.M. Cojocariu, P.H. Mutin, E. Dumitriu, F. Fajula, A. Vioux, V. Hulea, Chem. Commun. (Cambridge, U. K.), (2008) 5357-5359. http://dx.doi.org/110.1039/b811668g

[20] D.P. Debecker, K. Bouchmella, C. Poleunis, P. Eloy, P. Bertrand, E.M. Gaigneaux, P.H. Mutin, Chem. Mater., 21 (2009) 2817-2824. http://dx.doi.org/10.1021/cm900490t

[21] K. Bouchmella, P. Hubert Mutin, M. Stoyanova, C. Poleunis, P. Eloy, U. Rodemerck, E.M. Gaigneaux, D.P. Debecker, J. Catal., 301 (2013) 233-241. http://dx.doi.org/10.1016/j.jcat.2013.02.016

[22] V. Smeets, A. Styskalik, D.P. Debecker, J. Sol-Gel Sci. Technol., 97 (2021) 505-522. https://10.1007/s10971-021-05486-1

[23] D.P. Debecker, Chem. Rec., 18 (2018) 662-675. https://doi.org/10.1002/tcr.201700068

[24] N. Katada, H. Igi, J.-H. Kim, J. Phys. Chem. B, 101 (1997) 5969-5977. http://dx.doi.org/10.1021/jp9639152

[25] D.P. Debecker, K. Bouchmella, M. Stoyanova, U. Rodemerck, E.M. Gaigneaux, P. Hubert Mutin, Catal. Sci. Technol., 2 (2012) 1157-1164. http://dx.doi.org/10.1039/c2cy00475e

[26] K. Bouchmella, M. Stoyanova, U. Rodemerck, D.P. Debecker, P. Hubert Mutin, Catal. Commun., 58 (2015) 183-186. http://dx.doi.org/10.1016/j.catcom.2014.09.024

[27] G. Engelhardt, TrAC, Trends Anal. Chem., 8 (1989) 343-347. https://doi.org/10.1016/0165-9936(89)87043-8

[28] W. Lutz, D. Täschner, R. Kurzhals, D. Heidemann, C. Hübert, Z. Anorg. Allg. Chem., 635 (2009) 2191-2196. https://doi.org/10.1002/zaac.200900237

[29] X.S. Zhao, G.Q. Lu, A.K. Whittaker, G.J. Millar, H.Y. Zhu, J. Phys. Chem. B, 101 (1997) 6525-6531. http://dx.doi.org/10.1021/jp971366+

[30] W. Hu, Q. Luo, Y. Su, L. Chen, Y. Yue, C. Ye, F. Deng, Microporous Mesoporous Mater., 92 (2006) 22-30. https://doi.org/10.1016/j.micromeso.2005.12.013

[31] E. Lippmaa, A. Samoson, M. Magi, J. Am. Chem. Soc., 108 (1986) 1730-1735. http://dx.doi.org/10.1021/ja00268a002

[32] M.F. Williams, B. Fonfé, C. Sievers, A. Abraham, J.A. van Bokhoven, A. Jentys, J.A.R. van Veen, J.A. Lercher, J. Catal., 251 (2007) 485-496. https://doi.org/10.1016/j.jcat.2007.06.009

[33] T. Huang, Q. Peng, W. Shi, J. Xu, Y. Fan, Appl. Catal., B, 230 (2018) 154-164. https://doi.org/10.1016/j.apcatb.2018.02.053

[34] C. Jiménez-González, Z. Boukha, B. de Rivas, J.J. Delgado, M.Á. Cauqui, J.R. González-Velasco, J.I. Gutiérrez-Ortiz, R. López-Fonseca, Appl. Catal., A, 466 (2013) 9-20. https://doi.org/10.1016/j.apcata.2013.06.017

[35] M. Gil-Calvo, C. Jiménez-González, B. de Rivas, J.I. Gutiérrez-Ortiz, R. López-Fonseca, Appl. Catal., B, 209 (2017) 128-138. https://doi.org/10.1016/j.apcatb.2017.02.063

[36] N. Miletić, U. Izquierdo, I. Obregón, K. Bizkarra, I. Agirrezabal-Telleria, L.V. Bario, P.L. Arias, Catal. Sci. Technol., 5 (2015) 1704-1715. http://dx.doi.org/10.1039/C4CY01438C

[37] P. Burattin, M. Che, C. Louis, J. Phys. Chem. B, 101 (1997) 7060-7074. http://dx.doi.org/10.1021/jp970194d

[38] E. Heracleous, A.F. Lee, K. Wilson, A.A. Lemonidou, J. Catal., 231 (2005) 159-171. https://doi.org/10.1016/j.jcat.2005.01.015

[39] R. Hernández-Huesca, J. Mérida-Robles, P. Maireles-Torres, E. Rodríguez-Castellón, A. Jiménez-López, J. Catal., 203 (2001) 122-132. https://doi.org/10.1006/jcat.2001.3321

[40] S.R. Kirumakki, B.G. Shpeizer, G.V. Sagar, K.V.R. Chary, A. Clearfield, J. Catal., 242 (2006) 319-331. https://doi.org/10.1016/j.jcat.2006.06.014

[41] R. López-Fonseca, C. Jiménez-González, B. de Rivas, J.I. Gutiérrez-Ortiz, Appl. Catal., A, 437-438 (2012) 53-62. https://doi.org/10.1016/j.apcata.2012.06.014

[42] A.N. Mlinar, G.B. Baur, G.G. Bong, A.B. Getsoian, A.T. Bell, J. Catal., 296 (2012) 156-164. https://doi.org/10.1016/j.jcat.2012.09.010

Table 1: Experimental and nominal compositions of $Si_xAl_yNi_z$ samples.

Sample	Experimental / nominal composition (wt%) [a]			
	SiO_2	Al_2O_3	NiO	Si/Al [b]
$Si_0Al_{93}Ni_7$	0.0 / (0.0)	92.7 / (92.9)	7.3 / (7.1)	0
$Si_9Al_{84}Ni_7$	6.3 / (9.3)	86.5 / (83.6)	7.2 / (7.1)	0.1
$Si_{42}Al_{50}Ni_8$	40.5 / (42.4)	51.8 / (50.0)	7.7 / (7.6)	1
$Si_{80}Al_{12}Ni_8$	81.3 / (80.1)	12.4 / (12.0)	6.3 / (8.0)	8
$Si_{93}Al_0Ni_7$	92.2 / (92.7)	0.0 /(0.0)	7.8 / (7.3)	∞

[a] Experimental and nominal weight percentages (in brackets). Weight loadings are calculated from EDX results assuming that all Si, Al and Ni atoms are in the form of SiO_2, Al_2O_3 and NiO, respectively.
[b] Experimental atomic Si/Al ratio (EDX).

Table 2: Textural properties and the acidity of the $Si_xAl_yNi_z$ samples.

Sample	S_{BET} [a] ($m^2\ g^{-1}$)	Vp[b] ($cm^3\ g^{-1}$)	Dp[c] (nm)	Sμ[d] (nm)	Total acidity (mmol g^{-1})	Weak acidity (mmol g^{-1})	Medium-strong acidity (mmol g^{-1})
$Si_0Al_{93}Ni_7$	360	0.4	4.7	0	4.8	0.8	4.0
$Si_9Al_{84}Ni_7$	365	0.3	3.7	10	4.4	0.8	3.6
$Si_{42}Al_{50}Ni_8$	360	0.3	3.0	190	3.0	0.7	2.3
$Si_{80}Al_{12}Ni_8$	590	1.5	10.2	45	1.9	0.4	1.5
$Si_{93}Al_0Ni_7$	795	2.0	9.9	65	0.4	0.4	0

[a] Specific surface area determined by the BET method in the 0.05–0.25 P/P_0 range.
[b] Total pore volume at $P/P_0 = 0.98$.
[c] Average pore diameter 4 Vp/ S_{BET}.
[d] From *t*-plot analysis.

Table 3: Effect of reaction temperature on the catalytic performance of $Si_xAl_yNi_z$ catalysts.[a]

Catalyst	T (°C)	C2 conversion (%)	Product distribution (wt%)				Activity[c] (mmol g^{-1} h^{-1})
			C4	C6	C8	Other[b]	
$Si_{93}Al_0Ni_7$	150	15	90	8	1	1	54
	200	30	85	11	2	2	107
	250	43	78	15	4	3	154
	300	48	73	14	4	9	171
	350	55	57	10	3	30	196
$Si_{80}Al_{12}Ni_7$	150	40	83	11	3	3	143
	200	56	74	13	6	7	200
	250	76	54	19	12	15	271
	300	85	38	21	18	23	304
	350	95	21	18	15	46	339
$Si_{42}Al_{50}Ni_8$	150	66	75	15	13	2	236
	200	80	63	17	16	4	286
	250	85	50	20	22	8	304
	300	90	39	28	24	9	321
	350	95	34	23	19	22	339
$Si_9Al_{84}Ni_7$	150	76	71	18	8	3	271
	200	88	66	22	8	4	314
	250	92	63	24	9	4	329
	300	95	61	23	9	7	339
	350	96	27	5	1	67	343
$Si_0Al_{93}Ni_7$	150	77	69	10	6	15	275
	200	78	65	12	6	17	279
	250	80	60	14	7	19	286
	300	85	55	20	6	18	304
	350	92	27	3	1	69	329

[a] Reaction conditions: P = 3 MPa, WHSV = 10 h^{-1}, reaction time 1 h; [b]alkanes and uneven olefins; [c] average specific activity (mmol of C_2H_4 converted per gram of catalyst per hour)

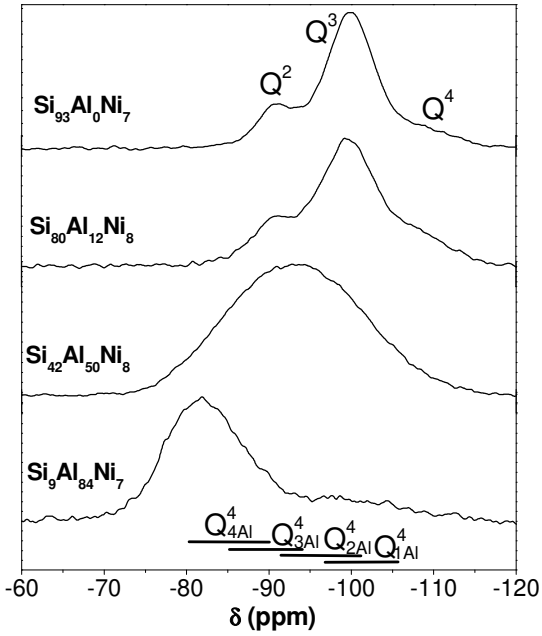

Figure 1: ^{29}Si CP-MAS NMR spectra of $Si_xAl_yNi_z$ samples.

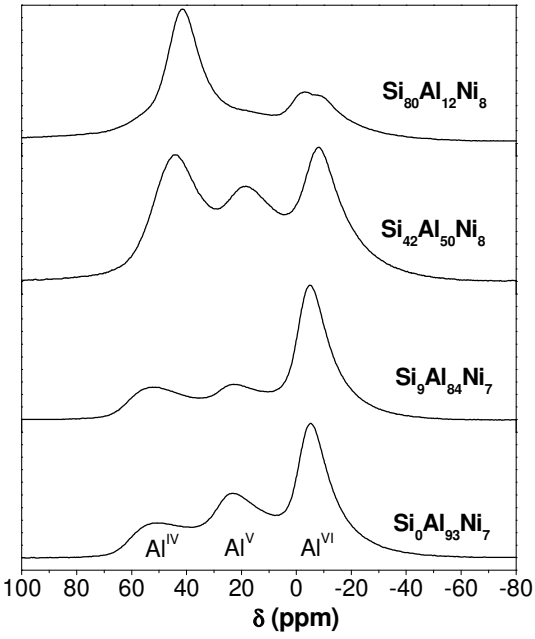

Figure 2: ^{27}Al MAS NMR spectra of $Si_xAl_yNi_z$ samples.

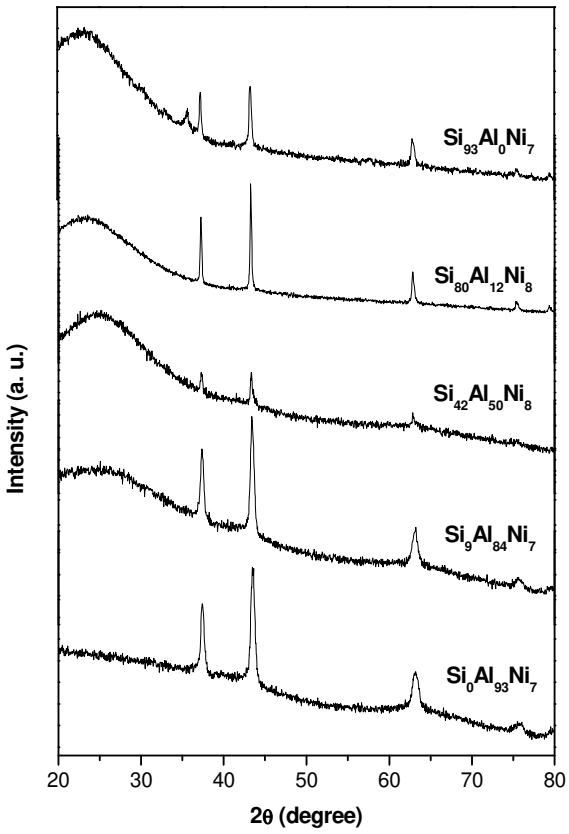

Figure 3: Powder XRD patterns of $Si_xAl_yNi_z$ samples.

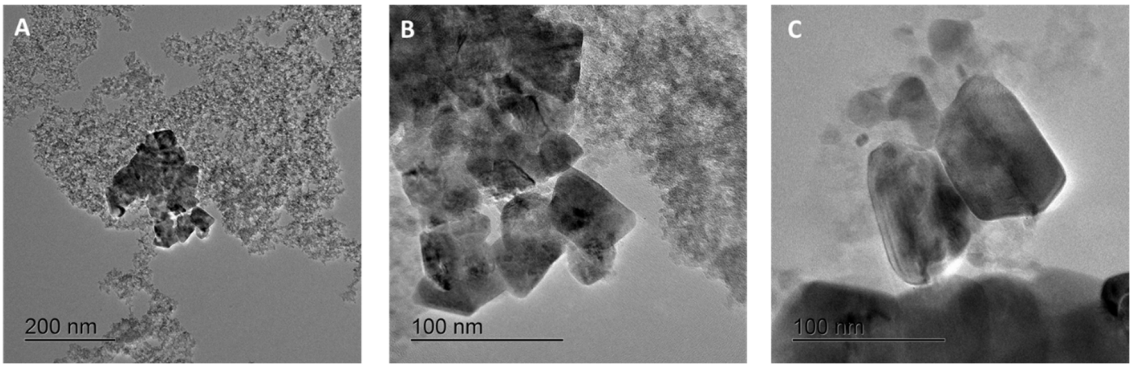

Figure 4: TEM images of $Si_{93}Al_0Ni_7$ showing the presence of aggregated NiO particles with a parallelepiped-like morphology.

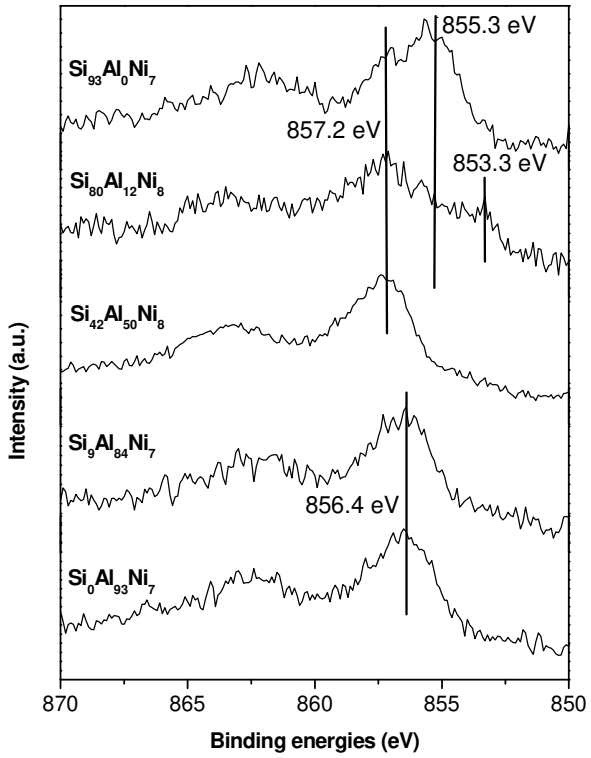

Figure 5: Ni2p3/2 XPS spectra of $Si_xAl_yNi_z$ samples.

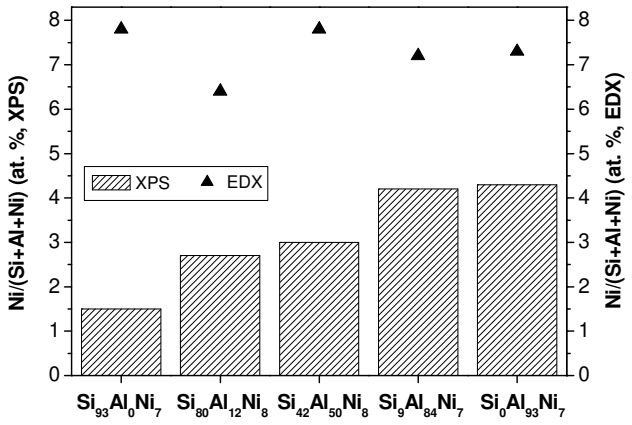

Figure 6: XPS (left axis, striped bars) and EDX (right axis, filled triangles) Ni/(Ni + Si + Al) atomic ratios for catalysts as a function of the Al_2O_3 weight loading.

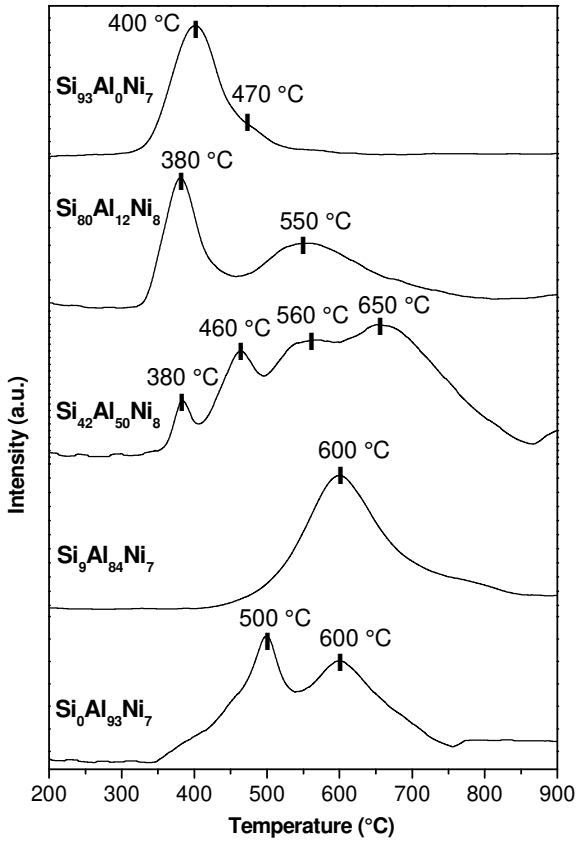

Figure 7: H_2-TPR profiles of $Si_xAl_yNi_z$ samples.

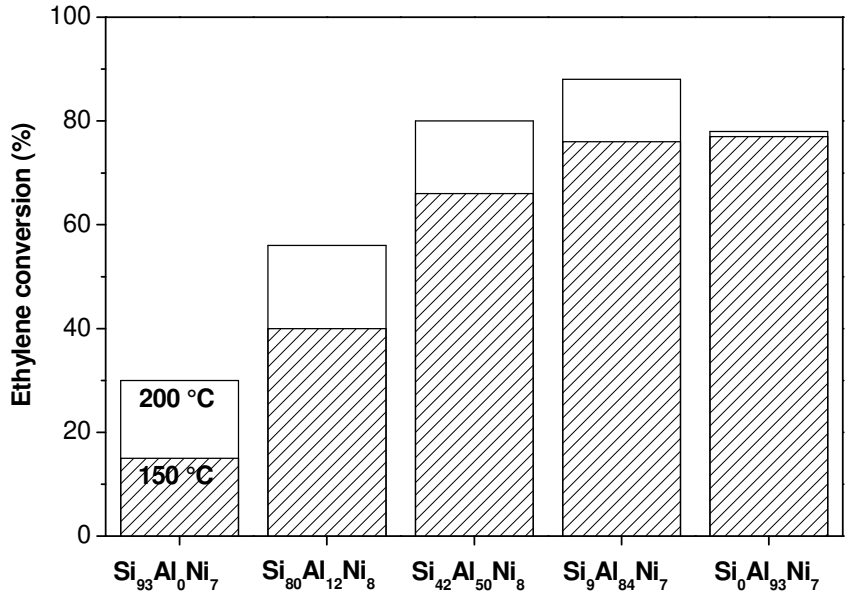

Figure 8: Ethylene conversion at 150 °C (striped bars) and 200 °C (empty bars) over the $Si_xAl_yNi_z$ catalysts.

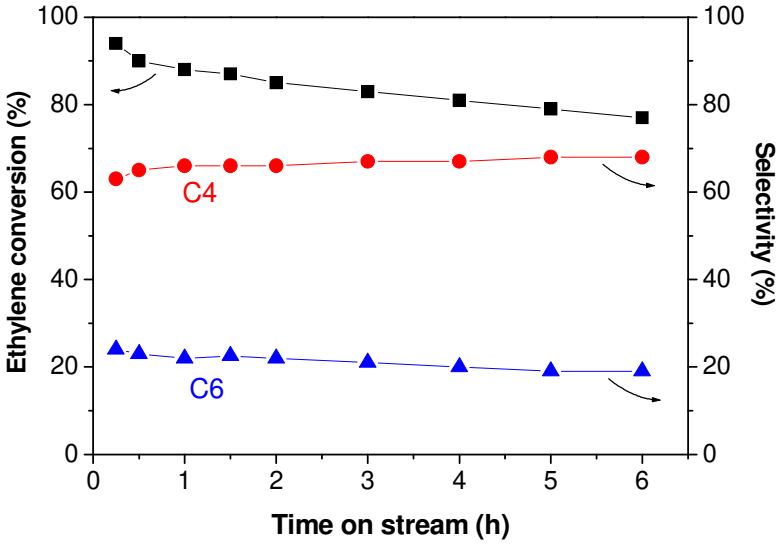

Figure 9: Ethylene conversion and C4/C6 selectivity vs. time on stream at 200 °C over the $Si_9Al_{84}Ni_7$ catalyst.

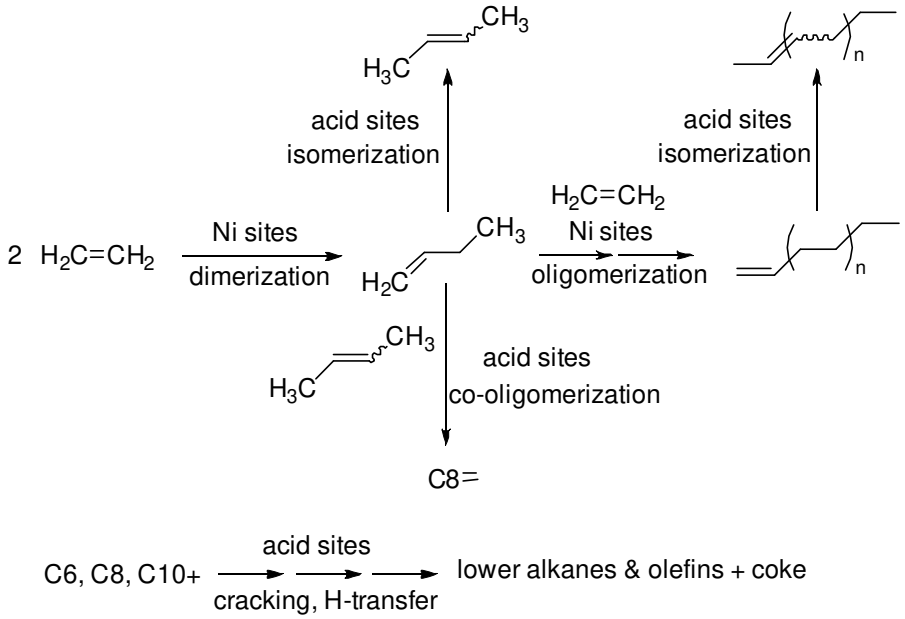

Scheme 1. Simplified scheme of the main reactions involved in ethylene oligomerization.

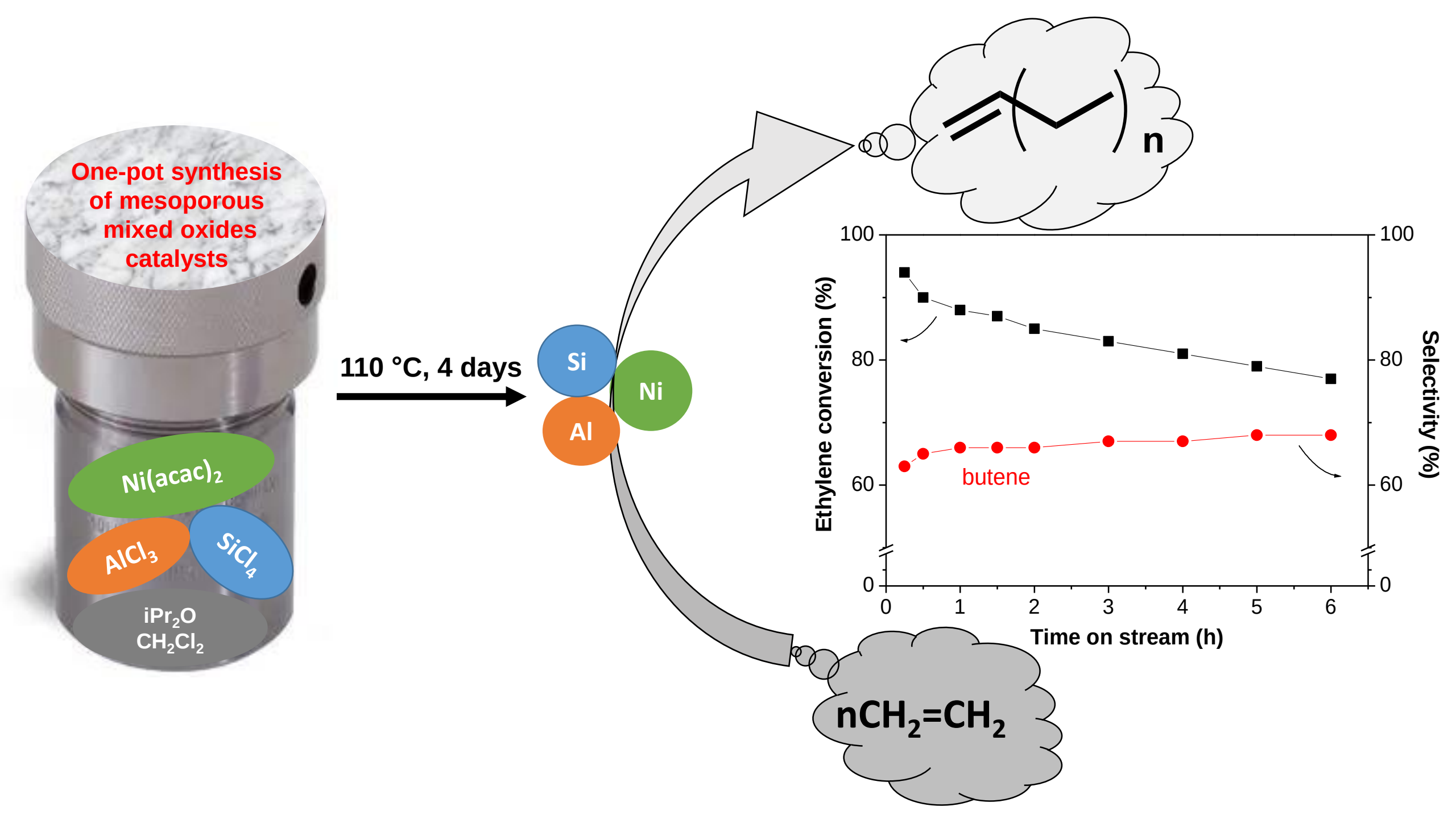
One-pot synthesis of mesoporous mixed oxides catalysts
Ni(acac)2
AlCl3
SiCl4
iPr2O
CH2Cl2
110 °C, 4 days
Si
Ni
Al
n
nCH2=CH2
Ethylene conversion (%)
Selectivity (%)
butene
Time on stream (h)
0
1
2
3
4
5
6
60
80
100